Heliyon 9 (2023) e12866

Contents lists available at ScienceDirect

Heliyon

journal homepage: www.cell.com/heliyon

Research article

Modification of bimetal Zn/ Mg MOF with nanoparticles Fe_3O_4 and $Fe_3O_4@SiO_2$, investigation of the peroxidase-like activity of these compounds by calorimetry and fluorimetry methods

Shaida Mahmoudi [a,b], Mohamad J. Chaichi [a,*], Mojtaba Shamsipur [b], O. Leila Nazari [a], Abdol R. Samadi Maybodi [a]

[a] Department of Analytical Chemistry, University of Mazandaran, Babolsar, Iran
[b] Department of Analytical Chemistry, University of Razi, Kermanshah, Iran

ARTICLE INFO

Keywords:
Datura
Composite
Peroxidase-like
Fluorometry
Calorimetry
Atropine

ABSTRACT

In this article; the bimetal metal-organic framework Zn/Mg (Zn/Mg MOF) is synthesized.

Then Zn/Mg MOF bimetal was combined with Fe_3O_4 and $Fe_3O_4@SiO_2$, and composites of $Fe_3O_4@$ SiO_2/MOF/Dextrin, $Fe_3O_4@SiO_2$/MOF, Fe_3O_4@MOF/Dextrin and Fe_3O_4@MOF made. The peroxidase-like activity of these compounds was investigated and compared by calorimetric Resazurin (Rz) and O-phenylenediamine (OPD); (Rz-H_2O_2, OPD-H_2O_2) and fluorimetric Rz and terephtalic acid (TA); (Rz-H_2O_2, TA-H_2O_2). The $Fe_3O_4@$ MOF/Dextrin composite has the highest peroxidase-like activity. The effect factors (amount of pH (6), the values of TA (1.37 mM), H_2O_2 (0.025 mM), reaction time (8.15 min), and amount of Composite (116.67 mg)) to increase the catalytic activity of $Fe_3O_4@$ MOF/Dextrin measured by chemometrics method. The most suitable linear range of the calibration curve by the TA-H_2O_2 -Composite fluorimetric method is 1–600 μg L^{-1}, and the detection limit is 2.27 μg L^{-1}. The relative standard deviation (RSD%) for measuring concentration atropine 1 μg L^{-1} (n = 6) is 1.18%. Finally, from this system for measuring atropine extracted by the Liquid-liquid extraction (LLE) method in two types of plants, D. Innoxia north and west and D. stramonium north and west of Iran (118.25 μg L^{-1}, 79.80 μg L^{-1}) and (18.477 μg L^{-1}, 9.27 μg L^{-1}) used, respectively.

1. Introduction

Datura is a well-known plant throughout history that grows naturally in temperate and arid regions. This plant from the Solanaceae family is rich in active chemicals such as phenolic, steroids, acyl sugars, amides, and alkaloids [1]. Tropane alkaloids (bicyclic [3.2.1] alkaloids) have given Datura its medicinal importance. Many studies have been done on this plant because alkaloids in specific doses have medicinal properties, in large quantities, are toxic, and lethal (The oral lowest toxic dose (TDLO) for atropine is 0.033 mg kg^{-1} in adults and 1.6–100 mg in children.) [2,3]. The most valuable tropane alkaloids are atropine (L-hyoscyamine) and scopolamine, which are very important in the pharmaceutical industry. Because atropine targets the parasympathetic nervous system to relieve pain, Anesthesia quit drug addiction, and control motor diseases is used [4,5]. To date, the main methods of measuring atropine have been chromatographic: Gas chromatography-mass spectroscopy (GC-MS) [1,2], liquid chromatography-MS [3-8], High-performance liquid

* Corresponding author. Department of Analytical Chemistry, University of Mazandaran, Babolsar, Iran.
E-mail address: jchaichi@yahoo.com (M.J. Chaichi).

https://doi.org/10.1016/j.heliyon.2023.e12866
Received 30 April 2022; Received in revised form 24 December 2022; Accepted 4 January 2023
Available online 7 January 2023

chromatography [9]. luminescence techniques [10-14].

Metal-organic frameworks (MOFs) or porous coordination polymers (PCPs) have individual properties of high porosity, several compositions, tunable pore structure, and multiple functionalities. Therefore, they have wide applications in different fields, especially catalysts [15]. Due to the weak coordinative bond between the metal and constituent ligand, the primary MOFs used as catalysts have limited mechanical, thermal, and chemical resistance [16,17]. Today, a type of functional materials (e.g., metal nanoparticles [NPs] [18-21], quantum dots [QDs] [22,23], polyoxometalates [POMs] [24,25], molecular species [26,27], enzymes [28,29], silica [30,31], and polymers [32-34] have been integrated with MOFs to generate MOF composites/hybrids composed. These composites have unique chemical and physical properties such as catalysis or peroxidase-like activity, optical, electrical, and magnetic properties, and mechanical strength [18]. Bimetallic systems have more catalytic activity than single-metal systems. The placement of secondary metal ions in the crystal lattices of metal oxides increases the optical, electrical, and magnetic properties by increasing the porosity and adsorption sites [35]. Until now, many studies have been done on the catalytic activity of Zn MOFs [36–38]. Nanoparticle Fe_3O_4 [39] inherently, and the composites obtained from Fe_3O_4 and MOFs have peroxidase-like active [39–42]. Other research to date has also been published mimicking the action of different composite MOFs of one metallic [43–45] and bimetallic [46–48]. Bimetallic Bi/Fe^0 is an active catalyst for the production of H_2 and the reduction of chloramphenicol in an aqueous environment [49]. Duped metals to TiO_2: Co–Fe–TiO_2 [50], Mn–Co–TiO_2 [51], and Phosphorous-Fluorine–Co-TiO_2 [35] used as photocatalysts in calorimetry peroxidase-like reactions. But so far, no article has been reported on the catalytic activity of peroxidase-like bimetallic hybrids Zn/Mg MOFs.

In this work, the peroxidase activity of composites Fe_3O_4@SiO_2/MOF/Dextrin(A), Fe_3O_4@SiO_2/MOF(B), Fe_3O_4@MOF/Dextrin(C), Fe_3O_4@MOF(D), Zn/Mg MOF(E) to measuring atropine in the Datura plant, investigated by fluorometric (TA-H_2O_2 and Rz) and colorimetric (OPD-H_2O_2) methods. Reactions in the presence of composite Fe_3O_4@MOF/Dextrin had the highest catalytic activity. Measure atropine by this catalyst, the amount of pH, the values of TA, H_2O_2, reaction time, and the amount of Composite were optimized to compound central design (CCD).

2. Experimental

2.1. Device and materials chemistry

Material used in the experiments were Magnesium nitrate hexahydrate ($Mg(NO_3)_2{\cdot}6H_2O$), zinc nitrate tetrahydrate ($Zn(NO_3)_2{\cdot}4H_2O$), terephthalic acid (TA), iron (II) chloride tetrahydrate ($FeCl_2{\cdot}4H_2O$), iron (III) chloride hexahydrate ($FeCl_3{\cdot}6H_2O$), tetraethyl orthosilicate (TEOS), sodium carbonate, epichlorohydrin, Hydrochloric acid (HCL) (37%), O-phenylenediamine (OPD), hydrogen peroxide (H_2O_2), Ammonia solution (32%), petroleum ethanol, Dimethylformamide (DMF), Dichloromethane (DCM), Dextrin were attained from Merck. Resazurin, Atropine, monosodium phosphate ($NaH_2PO_4{\cdot}H_2O$) were gained from Sigma.

In the Fourier transform infrared (FT-IR) spectroscopy, samples were operating with KBr tablets, measured by device an AVATAR spectrometer (Thermo, America).

Thermal gravimetric analyses (TGA) utilized the model STA 504 BAHR (Thermo Analyse, Germany) at a heating rate of 10 °C min^{-1}. We determined morphological characteristics by scanning electron microscopy, SEM (FEI, model Quanta 200, USA. Energy-dispersive X-ray spectroscopy (EDX) (device model: MIRA II, SAMX detector made in France, Czech Republic). Stable porosity of samples was investigated using adsorption and desorption isotherms of N_2 at 77K with device Brunauer–Emmett–Teller (BET) (device model: TriStar II PLUS, company of Micromeritics).

2.2. Preparation of Fe_3O_4 nanoparticles

22.5 mL of 0.12 M $FeCl_2{\cdot}4H_2O$ and 22.5 mL of 0.2 M $FeCl_3{\cdot}6H_2O$ solutions were blended in a 250 mL two-mouth flask. The total reaction system was ended under current nitrogen at 60 °C with a uniform speed of 15 min stirring. 21.6 mL of 3 M NaOH solution was added to the reaction system, and then reaction at 60 °C, 40 min was performed. Then stirred the reaction system at 90 °C for 30 min, and the resulting mixture cooled to room temperature. The dark sediment was assembled by magnetic and washed with deionized water/ethanol with (5:1v/v) three-time. The received dark residue dried over a vacuum at 30 °C overnight [38,52].

2.3. Preparation of Fe_3O_4@SiO_2

Modification of Fe_3O_4 Nanoparticles with TEOS: 30 mg of Fe_3O_4 synthesized acidized by HCl (0.1 mol L^{-1}) ultrasonic for 20 min. Using a magnet, discard the supernatant; the residual was washed with H_2O three times, then added H_2O/ethanol (60:40 v/v) was to sample that magnetic nanoparticles suspension. Ammonia (750 μL) was added to Fe_3O_4, and the compound was reacted with for 20 min under the ultrasound at 40 °C. TEOS (96 μL) was attached to the samples. Then the examples oscillated at 140 min^{-1} for 3 h, magnetic nanoparticles sorption by the magnet. The supernatant was thrown away, and the sediment was washed with H_2O/ethanol three times to yield Fe_3O_4@SiO_2 [53].

2.4. Synthesis of bimetal Zn/Mg MOF

To synthesize Zn/Mg MOF (Zn:Mg ratio of 1:1), dissolve 1.8 g $Zn(NO_3)_2{\cdot}4H_2O$, 1.5 g $Mg(NO_3)_2{\cdot}6H_2O$, and 1.7 g TA in 80 ml DMF for 15 min, add 0.5 ml Hydrochloric acid (3 mmol) to the solution and after 60 min stirring, mix for 24 h at 120 °C in the autoclave.

Cool the sample gently at room temperature. Separate the solvent from the sediment by centrifugation (8000 rpm, 10 min), wash the precipitate twice with H_2O and ethanol for 12 h, and finally store in ethanol for 24 h. Then collect the precipitate Zn/Mg MOF by centrifugation and dry overnight in a vacuum oven (37 °C).

2.5. Preparation of hybrids Fe_3O_4@SiO_2/MOF, Fe_3O_4@MOF

These composites were synthesized: 0.05 g Fe_3O_4@SiO_2 or Fe_3O_4, 0.5 g $Mg(NO_3)_2{\cdot}6H_2O$, 0.5 g $Zn(NO_3)_2{\cdot}4H_2O$ in 40 ml DMF were ultrasonic for 60 min Then solution TA (0.5 g TA+ 40 ml DMF) was added to it, and 24 h at 120 °C in autoclave then precipitated slowly at room temperature, centrifugation precipitate and washed twice for 12 h with DMF washes. Precipitation was collected by centrifugation and dried in a vacuum oven for 24 h, 36 °C.

2.6. Synthesis of hybrids Fe_3O_4@SiO_2/MOF/dextrin, Fe_3O_4@MOF/dextrin

TO synthesize these composites, 0.5 g Fe_3O_4@SiO_2/MOF or Fe_3O_4@MOF, 40 ml DMF, 1.2 g Dextrin, 4 g sodium carbonate, and 0.6 g cross-linker epichlorohydrin under nitrogen gas, 85 °C, 24 h reaction performed. The product is cooling to room temperature. The precipitate is filtered and washed 3 with DMF and THF and dried in a vacuum oven (50 °C).

2.7. Synthesis of MOF-5 and Mg-MOF

0.5 g $Zn(NO_3)_2{\cdot}4H_2O$ or $Mg(NO_3)_2{\cdot}6H_2O$ in 20 ml DMF ultrasonic 30 min, then solution TA (0.25 g TA+ 20 ml DMF) was added to it, and 24 h at 120 °C in autoclave then precipitation cooling at room temperature. Centrifugation precipitation and washed twice for 12 h with DMF washes. Precipitate collected by centrifugation and dried in a vacuum oven for 24 h, 36 °C.

2.8. Preparation of datura sample

0.5 g of dried defatted samples dissolved in 30 ml methanol for 60 min. The extract filtration by paper. The solvent removes by rotary; The temperature should not exceed 40 °C. 5% hydrochloric acid (50 ml) added to the flask containing the dried extract during sonication. The aqueous acid phase was extracted with 3 × 40 mL DCM. The organic phase was discarded at the bottom of the decanter. The pH of the aqueous phase was adjusted to pH 10 with ammonium hydroxide 25%, Then the Atropine was extracted with 5 × 40 mL of DCM. The organic phase was separated and dried with 30 g of anhydrous sodium sulfate. The dry extract of Atropine was solubilized in 1 ml H_2O.

2.9. Fluorometric experiments of TA-H_2O_2

Atropine has a decreasing effect on the fluorescence resulting from the catalytic activity of all synthesized composites. The atropine in Datura was measured, using this effect decreasing. Initially, each sample has a certain amount of composites. The specific concentration of TA dissolved in 2 ml PBS (0.01 M, definite pH), 50 μl of H_2O_2 with specific concentration, 100 μl of PBS (0.01 M), and 1 ml of atropine.

Shake the final sample with a constant volume of 3.2 ml at room temperature in a dark environment for a specific reaction time. Composites separated by centrifugation (8000 rpm, 10 min), then a difference in fluorescence intensity ($F=F_0 - F_a/F_0$; F_0 and F_a are related to the fluorescence intensity of the sample in the absence and presence of atropine.) of the high clear solution was recorded at wavelength emission 450 nm and excitation 315 nm.

2.10. Optimization of composite mimetic activity conditions in TA-H_2O_2 system

Response surface methodology (RSM) is a set of experimental design (DOE) techniques that help researchers better understand and optimize laboratory responses. Central composite design (CCD) is the most common RSM experiment and is suited to the quadratic model.

The highest mimetic activity of the composite has five effect factors (amount of composites, pH, concentration H_2O_2 and TA, reaction time) in the reaction optimized. Factor optimization was done by CCD/half fractional factorial (HFF) using Minitab 17 software.

Table 1
Experimental variables and levels of the CCD.

Factors	Unit	Levels	
		Low (−1)	High (+1)
pH (X_1)		**7**	**9**
concentrations TA(X_2)	**-mM**	**1**	**2**
concentrations H_2O_2(X_3)	**mM**	**0.015**	**0.03**
amount of composites (X_4)	**Mg**	**100**	**200**
reaction time (X_5)	**Min**	**5**	**12**

Table 1 shows experimental variables and levels of the CCD.

2.11. Calorimetry test of OPD-H_2O_2

For the OPD-H_2O_2 calorimetry test, 1.5 ml of OPD (5 mM), 1.5 ml of composite 250 mg, and 200 μl of atropine (100 μg ml^{-1}) dissolve in acetate buffer (pH = 4, 0.01 M) and then add 300 μl of H_2O_2 (1 mM) to the solution and increase the volume of the final solution to 3.5 ml. The reaction was completed for 20 min incubated in a dark room. Then the composites were separated using a centrifuge (10 min, 6000 rpm), and the adsorption of a high clear solution at λabs = 445 nm by The UV–vis device was measured.

2.12. Calorimetry and fluorimetry test of Rz-H_2O_2

Dissolved 1.5 ml of Rz (2.5 μM) in phosphate buffer (pH = 6.5, 0.01 M), 1.5 mM composite 250 mg, dissolved 200 μL of atropine (100 μgml-1) in phosphate buffer (pH = 8, 0.01 M), then add 300 μl of H_2O_2 (1 mM) solution add the volume of a final solution to 3.5 ml Complete the reaction 1 h incubated in the dark room. Then separated the composites using a centrifuge (10 min, 6000 rpm). And finally, absorb the color of the high transparent solution in λ_{abs}, Rz = 601 nm and λ_{abs}, Resorufin (Rf) = 573 nm by Uv–vis and Rf fluorescence at λ_{ex} = 530 nm and λ_{em} = 590 nm Was measured.

3. Result and discussion

3.1. Characteristics of synthesized composites of MOF

Fig. 1 shows the spectrum obtained from FT-IR for bimetallic MOF and MOF-derived composites. The scattering of the Zn/Mg bimetallic MOF peaks according to Ref. [39] in the range 470–1700 cm^{-1} is observable. The sharp and weak peaks in the region of 427–527 cm^{-1} correspond to the oxides of Zn–O and Mg–O metals attached to the ligand, respectively. The peaks in the 685–826 cm^{-1} region are related to the bending vibrations of the C–H ring-in-and-out bond in TA. The sharp peaks in 1546–1698 cm^{-1} and 1383-1439 cm^{-1} describe asymmetric and asymmetric stretching vibrations of the carboxyl group in the TA ligand bridged between Mg and Zn. Very weak peaks in the 2583 and 3098 cm^{-1} regions belong to the methyl group in the DMF solvent. The weak peak in the area of about 2000 cm^{-1} is related to the metal Mg attached to TA. this peak is very weak and indicates the connection of a small percentage of metal Mg is with TA, and a higher percentage of Mg is associated with TA which acts as a bridge between the two metals Mg and Zn [40]. All spectra except MOF, approximately wide peaks in the region of 3400 cm^{-1} and 495-598 cm^{-1} interrelated to the stretching vibrations of O–H and Fe–O, respectively. In composites containing SiO_2 in the range of 2900 cm^{-1}, 950 cm-1, 1024 and 750-800 cm^{-1}, near 492 cm^{-1}, It is related to aliphatic C–H bond in methyl and propyl groups, Si–OH, Si–O–Si, and Fe–O–Si, respectively.

The peaks seen in the range of 3000 cm-1, 1300 cm^{-1}, and 1180 cm^{-1} are related to the stretching vibrations of C–H aromatic, C–C, and C–O related to Dextrin, respectively, which are well in the range of composites with Dextrin seen.

Morphological surface, porous structure of materials, composite sizes checks using the scanning electron microscope. Fig. 2(a–e) shows a clear picture of SEM for Zn/Mg bimetal MOFs and their composites. These composites have an irregular but porous structure.

Fig. 3 shows the TGA curve for composites synthesized from A-E. For composite A at 112.8–184.8 °C, B at 103.3–274.4 °C, D at 77–240 °C and E at 110–175 °C represents A-E with weight loss of 16.85%, 21%, 26.81%, 24.3%, 11.33% for solvent, respectively. With increasing temperature, degradation of the ligand and the structure of the composites from A-E at temperatures above 370 °C, 420 °C, 460 °C, 350 °C and 340 °C performed.

Fig. 4(A–D) demonstrates the composites and MOF bimetal elemental analysis energy-dispersive X-ray spectroscopy (EDX). In this

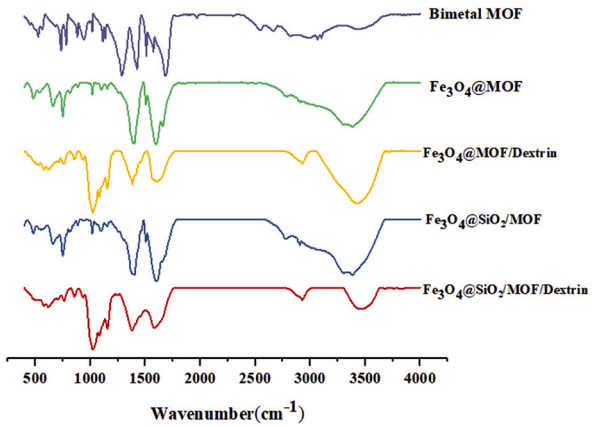

Fig. 1. FT-IR spectra of bimetal MOF and composites synthesized.

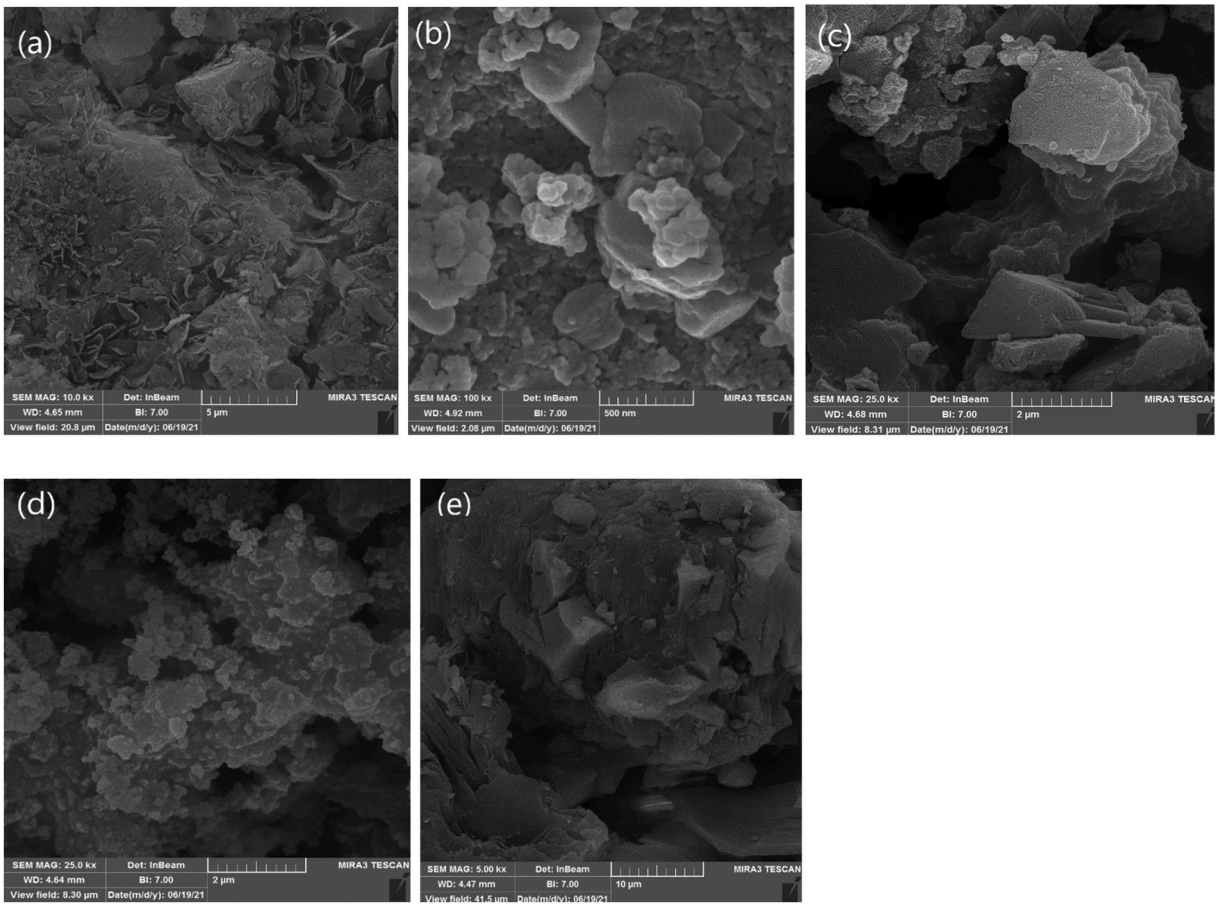

Fig. 2. SEM images of a) Fe_3O_4@SiO_2/MOF/Dextrin, b) Fe_3O_4@SiO_2/MOF, c) Fe_3O_4@MOF/Dextrin, d) Fe_3O_4@MOF, e) Zn/Mg bimetallic produced.

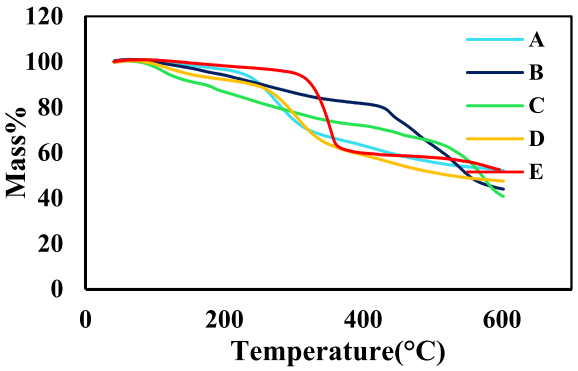

Fig. 3. TGA curves of composites synthesis A-E.

analysis, the ratio of Zn to Mg for A-D composite and bimetal MOF is 4.51: 3.7, 6.32: 7.57, 3.05: 2.51, 6.9: 7.63, 5.77: 4, respectively. Confirms the ratio of Zn to Mg atoms of approximately 1:1 in these composites.

Table 2 shows the surface area, pore volume, and pore diameter BET for the composites. The observed decrease in surface area E to A composite is due to the closure of the pores in the MOF bimetallic by molecules Dextrin and SiO_2.

3.2. Optimization of composite MOF mimetic activity conditions

The main factors were optimizing through CCD/HFF. In the method, factors were defining in two levels of (−1, +1), including 32 runs with α= 2.

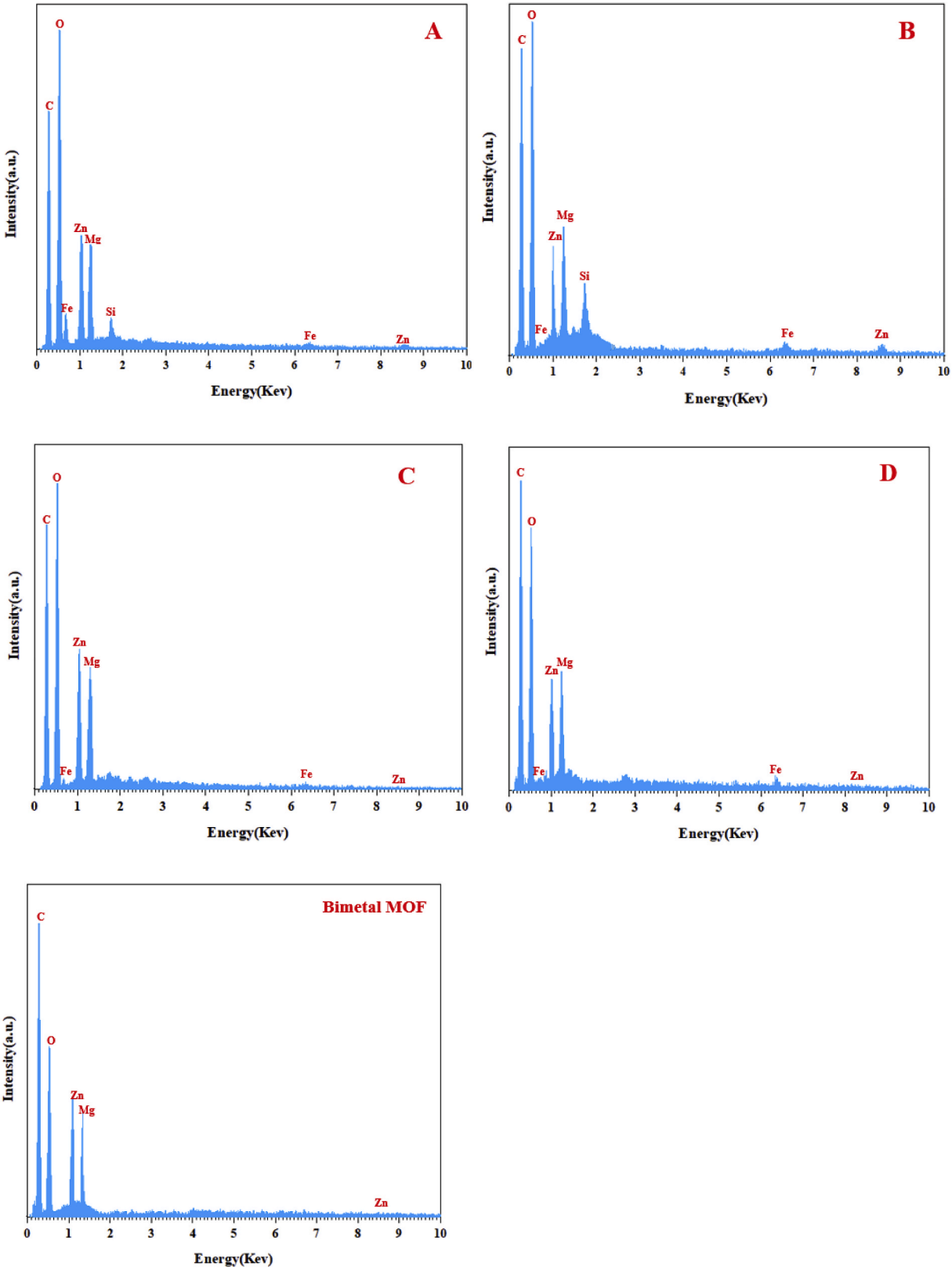

Fig. 4. EDX related to composites A-D and bimetal MOF.

Table 2
BET specifications for composites.

Composite	surface area ($m^2\ g^{-1}$)	pore volume ($cm^3\ g^{-1}$)	pore diameter (nm^2)
A	358.586	0.00061	0.160
B	361.442	0.15613	0.160
C	397.000	0.22860	0.160
D	422.6641	0.13504	0.160
E	746.157	0.31548	0.160

Table 3 exhibits the matrix of the CCD design experiments for five effect factors. Analysis of the variance (ANOVA) shows the suitability of the experimental data to the response surface model (Table 4).

Based on the results ANOVA p-value <0.05 significant parameters indicate a 95% confidence level. R^2 and R^2-adjusted for the model are 99.97 and 99.92%, respectively. These data confirm the value accuracy and correlation between the predicted responses and the experimental data obtained. The lack of fit (LOF) p-value is 0.094, less than 0.05%, which indicates the compatibility of the model with the data. The regression equation for this model is as follows, the model includes the main factors and binary interaction between the main factors:

$$F = 634.8–340.7\ X_1 + 395.6\ X_2 + 37264\ X_3 + 1.997\ X_4 + 86.88\ X_5 + 9.629\ X_1^2 – 222.38\ X_2^2 – 643908\ X_3^2 – 0.020575\ X_4^2 – 5.5125\ X_5^2 + 24.23\ X_1X_2 – 197 \times 1 \times 3 + 0.5564 \times 1 \times {}_4 + 1.183 \times 1 \times 5 + 1603 \times 2 \times {}_3 + 0.0449 \times 2 \times 4 + 3.116 \times 2 \times 5 – 28.20 \times 3 \times 4 – 365.1 \times 3 \times 5 + 0.00793 \times 4 \times 5$$

Fig. 5 shows optimal values predicted for effective factors by RSM, in which the maximum response to the catalytic activity composite is predicted. Based on these results, the optimal values are for pH = 6, the concentration TA = 1.37 mM and H_2O_2 = 0.025 mM, amount of MOF = 116.67 mg, reaction time = 8.15 min. Fig. 6 displays the response surface diagram for each pair of factors.

Table 3
The matrix of the CCD design experiments.

Factor	Levels						
	-α		−1	0		+1	+α
	−2		−1	0		1	**2**
X_1	6		7	8		9	**10**
X_2	0.5		1	1.5		2	**2.5**
X_3	0.0075		0.015	0.0225		0.03	**0.0375**
X_4	50		100	150		200	**250**
X_5	1.5		5	8.5		12	**15.5**
Run	X1	X_2	X_3	X_4	X_5	**Flu. intensity**	
1	**0**	**0**	**0**	**0**	**0**	**261.12**	
2	**−1**	**−1**	**1**	**1**	**1**	**78.923**	
3	**1**	**1**	**−1**	**−1**	**1**	**−21.900**	
4	**1**	**−1**	**1**	**1**	**−1**	**11.515**	
5	**0**	**-α**	**0**	**0**	**0**	**42.460**	
6	**0**	**0**	**0**	**0**	**+α**	**−9.080**	
7	**−1**	**1**	**1**	**1**	**−1**	**81.070**	
8	**−1**	**−1**	**1**	**−1**	**−1**	**215.154**	
9	**1**	**−1**	**−1**	**1**	**1**	**23.502**	
10	**-α**	**0**	**0**	**0**	**0**	**424.107**	
11	**0**	**0**	**+α**	**0**	**0**	**142.082**	
12	**−1**	**1**	**−1**	**−1**	**−1**	**97.665**	
13	**0**	**0**	**0**	**-α**	**0**	**79.022**	
14	**1**	**−1**	**1**	**−1**	**1**	**−18.923**	
15	**0**	**0**	**0**	**0**	**0**	**258.804**	
16	**0**	**+α**	**0**	**0**	**0**	**32.703**	
17	**1**	**1**	**1**	**−1**	**−1**	**16.194**	
18	**−1**	**1**	**−1**	**1**	**1**	**68.370**	
19	**+α**	**0**	**0**	**0**	**0**	**172.849**	
20	**0**	**0**	**-α**	**0**	**0**	**88.08**	
21	**1**	**1**	**1**	**1**	**1**	**34.095**	
22	**−1**	**−1**	**−1**	**−1**	**1**	**156.835**	
23	**0**	**0**	**0**	**0**	**-α**	**−11.222**	
24	**0**	**0**	**0**	**0**	**0**	**263.889**	
25	**0**	**0**	**0**	**0**	**0**	**259.711**	
26	**1**	**−1**	**−1**	**−1**	**−1**	**−48.741**	
27	**0**	**0**	**0**	**0**	**0**	**258.053**	
28	**1**	**1**	**−1**	**1**	**−1**	**−4.823**	
29	**0**	**0**	**0**	**0**	**0**	**260.572**	
30	**−1**	**−1**	**−1**	**1**	**−1**	**96.510**	
31	**−1**	**1**	**1**	**−1**	**1**	**162.678**	
32	**0**	**0**	**0**	**+α**	**0**	**29.400**	

Table 4
ANOVA table from RSM.

Source	Df	Sum of squares	Mean square	F- value	P-value	
Model	20	410574	20529	2037.02	0.000	Significant
Linear	5	81006	19531	1938.02	0.000	Significant
$\mathbf{X_1}$	1	89891	89891	8919.66	0.000	Significant
$\mathbf{X_2}$	1	425	425	42.13	0.000	Significant
$\mathbf{X_3}$	1	4301	4301	426.8	0.000	Significant
$\mathbf{X_4}$	1	3016	3016	299.27	0.000	Significant
$\mathbf{X_5}$	1	23	23	2.25	0.162	Insignificant
Square	5	293515	58703	5824.96	0.000	Significant
$\mathbf{X_1^2}$	1	2720	2720	269.90	0.000	Significant
$\mathbf{X_2^2}$	1	90663	90663	8996.23	0.000	Significant
$\mathbf{X_3^2}$	1	38482	38482	3818.44	0.000	Significant
$\mathbf{X_4^2}$	1	77610	77610	7701.06	0.000	Significant
$\mathbf{X_5^2}$	1	133760	133760	13272.71	0.000	Significant
2-Way Interaction	10	19404	19404	192.55	0.000	Significant
$\mathbf{X_1X_2}$	1	2349	2349	233.05	0.000	Significant
$\mathbf{X_1X_3}$	1	35	35	3.45	0.090	Insignificant
$\mathbf{X_1X_4}$	1	12383	12383	1228.75	0.000	Significant
$\mathbf{X_1X_5}$	1	274	274	27.20	0.000	Significant
$\mathbf{X_2X_3}$	1	578	578	57.35	0.000	Significant
$\mathbf{X_2X_4}$	1	20	20	2.00	0.185	Insignificant
$\mathbf{X_2X_5}$	1	476	476	47.20	0.000	Significant
$\mathbf{X_3X_4}$	1	1789	1789	177.55	0.000	Significant
$\mathbf{X_3X_5}$	1	1470	1470	145.85	0.000	Significant
$\mathbf{X_4X_5}$	1	31	31	3.06	0.108	Insignificant
Residual	11	111	10	–	–	Significant
Lack-of-Fit	6	90	15	3.52	0.094	–
Pure Error	5	21	4	–	–	–
Total	31	410685	–		–	

3.3. Mechanism of the peroxidase-like activity of composite and fluorometric studies TA- H_2O_2

An indirect probe TA- H_2O_2 was used to detect OH° to investigate the catalytic activity of the synthesized composites. In the presence of TA- H_2O_2 alone, no emission for fluorescence is visible.

At the present atropine, the catalyst is a possible mechanism, H_2O_2 collides with sites active in the composite converted to hydroxide radicals (OH°). TA reacts with OH° to produce 2-hydroxy terephthalic acid (2-HTA). This compound is excited at $\lambda_{ex} = 315$ nm and has an intense fluorescence at $\lambda_{em} = 425$ nm. Fig. 7 shows the results for comparing peroxidase-like activity for different synthesized composites. The results record that the highest mimetic activity is related to Fe_3O_4@MOF/Dextrin composite. This increase is due to the synergistic effect of diffuse iron ions between Zn and Mg metals in the MOF and dextrin layers. The synergistic effect increases the high surface area and numerous sites in the composite, creating an intensely mimetic activity to reduce H_2O_2 lowest increase in catalytic activity is related to composites with SiO_2 coating. This decrease is due to the reduction of Fe_3O_4 active sites by SiO_2 particles, which reduces the synergistic effect of iron ions on the catalytic activity of the composite.

3.4. Calorimetry test of OPD-H_2O_2

OPD is a peroxidase for the OH° probe by calorimetric testing. In this experiment, OPD reacts with H_2O_2 to form the yellow substance 2,3-diaminophenazine (DAP), adsorbed in the 445 nm region. Fig. 8 shows the catalytic activity of composites in the presence of OPD-H_2O_2. The Fe_3O_4@MOF/Dextrin composite has the highest adsorption.

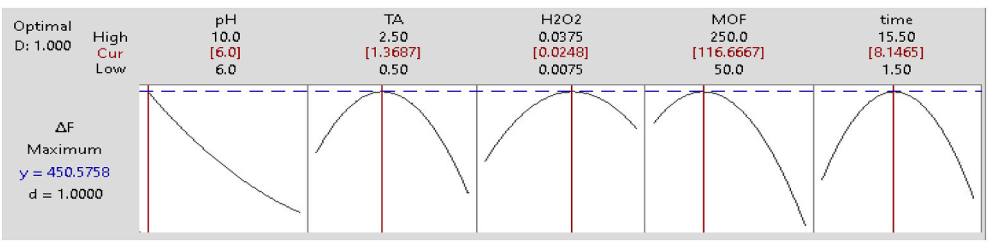

Fig. 5. Optimal values predicted for effective factors by RSM.

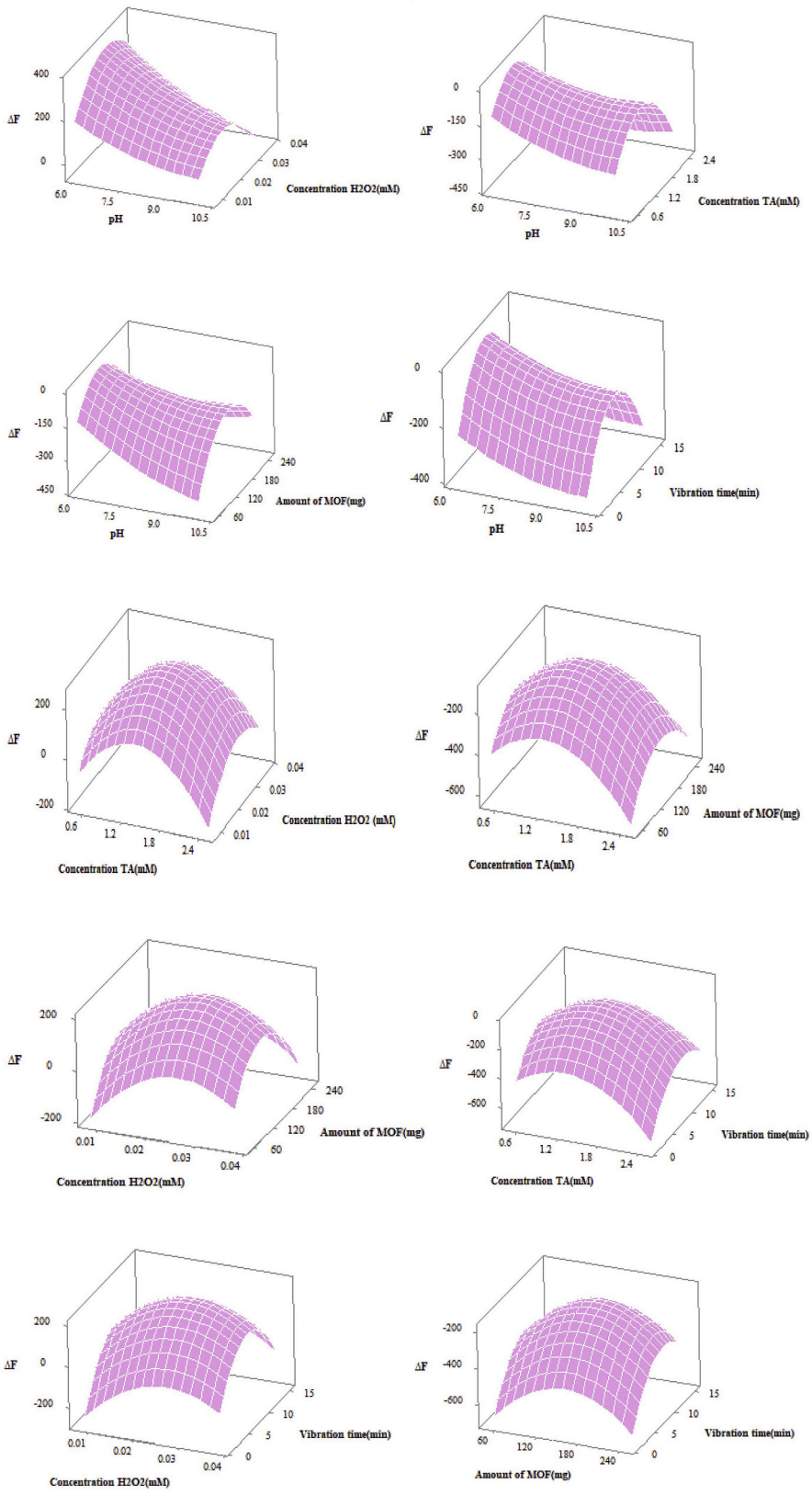

(caption on next page)

Fig. 6. Display the response surface diagram for each pair of factors.

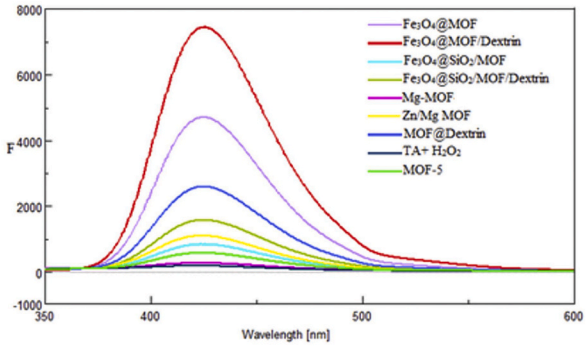

Fig. 7. Shows the results for comparing peroxidase-like activity for different synthesized composites.

3.5. Calorimetry and fluorimetry test of Rz-H_2O_2

Rz-H_2O_2 was used to evaluate the catalytic activity of composites induced by free or surface electrons prepared for peroxidase reactions. Reduction of Rz in two forms of calorimetry by changing the blue color (λ_{abs} = 601 nm, Rz) to pink (λ_{abs} = 573 nm, Rf) (Fig. 9a) and fluorimetry with high emission of fluorescence Rf to weak emission of Rz (Fig. 9b). In this test, the high catalytic activity of Fe_3O_4@MOF/Dextrin composite was well demonstrated.

3.6. Method validation

Validation of the method was determined through parameters linear ranges (LRs), determination coefficient (R2), relative standard deviations (RSDs), the limit of detection (LOD), and the limit of quantification (LOQ).

First, the atropine calibration curve in solutions with standard concentrations (1–600 μg L^{-1}) plotted by the peroxidase-like activity of the Fe_3O_4@MOF/Dextrin composite based on the fluorimetric experiment in Fig. 10.

The linear range for measuring atropine is approximately 1–600 μg L^{-1}. Regression equation F = 1.2981C + 10.037 (slope of calibration curve m = 1.2981, the standard deviation of S_b blank solution with concentration 1 μg L^{-1} for six repetitions in measuring fluorescence intensity 1.18% Was registered).

LOD, LOQ and R^2 were calculated to be 2.27 μg L^{-1}, 9.09 μg L^{-1} and 0.9974, respectively. Finally, atropine extracted by the LLE method from the seeds of two types of D. innoxia and D. Stramonium native to the north and west of Iran was measured by this method. The results obtained for sample D. Innoxia north and west of Iran and D. stramonium north and west of Iran were published 118.25 μg L^{-1}, 79.80 μg L^{-1}, 18.477 μg L^{-1}, 9.27 μg L^{-1}, sequentially.

3.7. Selectivity and stability of the catalytic activity of the composite

Selectivity, stability, and repeatability are important offices of the fluorescence method in measuring specific analytes. Selectivity and stability indicate the practicality of selecting and resisting the catalyst in measuring the desired analyte in an environment containing different compounds. The selectivity of this method was investigated by fluorescence response to TA-H_2O_2–Fe_3O_4@MOF/Dextrin composite system for different species in the presence or absence of atropine. In Fig. 11, the selectivity of this method for

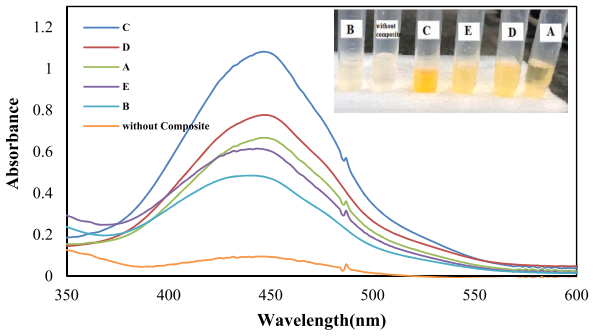

Fig. 8. Absorption spectra of OPD (5 mM)-H_2O_2(1 mM) solution after exposing to different MOFs (250 mg L^{-1}, [Buffer:0.01 M acetate, pH 4]).

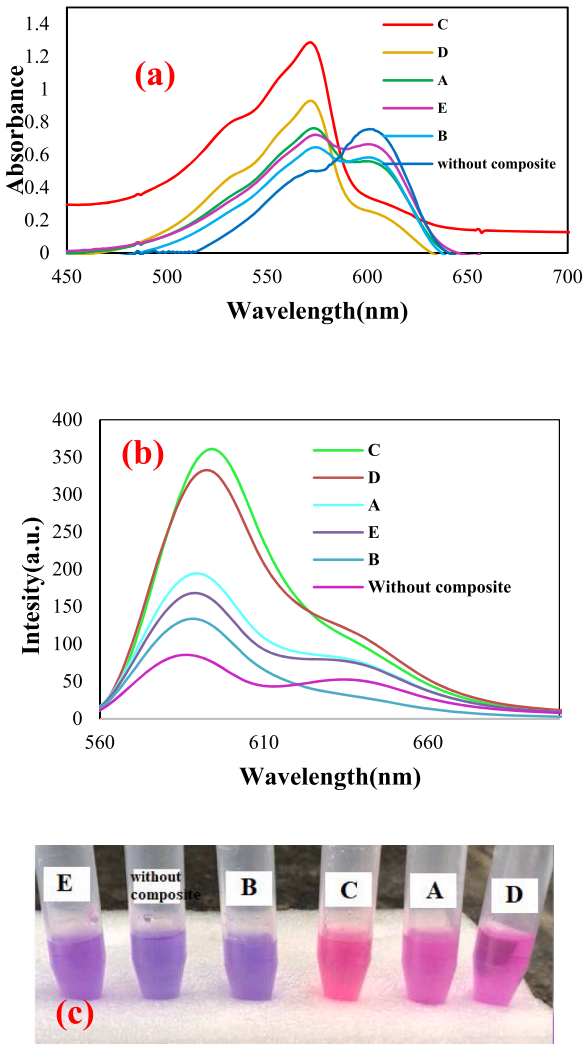

Fig. 9. a) Absorption spectra, b) fluorescence spectra, c) Color change Rz in the presence of composites; of Rz (25 μM)-H_2O_2(1 mM) solution after exposing to different MOFs (250 mg L^{-1}, [Buffer:0.01 M phosphate, pH 8].

estimating atropine is well evident. In the absence of atropine, the fluorescence intensity of all compounds is approximately identical but decreases with AT fluorescence.

After the reaction of TA–H_2O_2–Fe_3O_4@MOF/Dextrin composite system, evaluating the stability and repeatability of bimetal MOF, the composites was separated from the solution using a centrifuge (8000 rpm, 8 min). MOF was washed five times with methanol: H_2O (4:1 v/v), then dried overnight at 37 °C temperature in a vacuum oven. The composites were used again for the same reaction. This cycle was repeated 10 times. The composites have nearly the same responses for five thighs. It can be recoverable with the same sensitivity for five thighs and gradually lose its proficiency.

Activity efficiencies for thighs 6, 8, and 10 are 89.46%, 75.5% and 37.2% individually.

4. Conclusions

One of the main methods to increase the catalytic activity of MOFs is to merge them with applied materials and produce composites. This work synthesized Zn/Mg bimetallic MOF with the terephthalic acid ligand. Composites integrated with this bimetallic MOF: Fe_3O_4@SiO_2/MOF/Dextrin, Fe_3O_4@SiO_2/MOF, Fe_3O_4@MOF/Dextrin, Fe_3O_4@MOF. The peroxidase-like activity of these compounds was investigated and compared by calorimetry (Rz-H_2O_2, OPD-H_2O_2) and fluorimetry (Rz-H_2O_2, TA-H_2O_2). Atropine has a reducing effect on the catalytic activity of these compounds. The greatest effect was reported for Fe_3O_4@MOF/Dextrin composite in all colorimetric and fluorimetric tests. Optimized factors the amount of pH (6), the values of TA (1.38 mM), H_2O_2 (0.026 mM), reaction time (8.2 min), and amount of Composite (122.72 mg) to increase the efficiency of Fe_3O_4@MOF/Dextrin composite was improved for Datura plant atropine quantity by TA-H_2O_2 system using CCD method. This system is a highly selective, sensitive, quick, and reversible

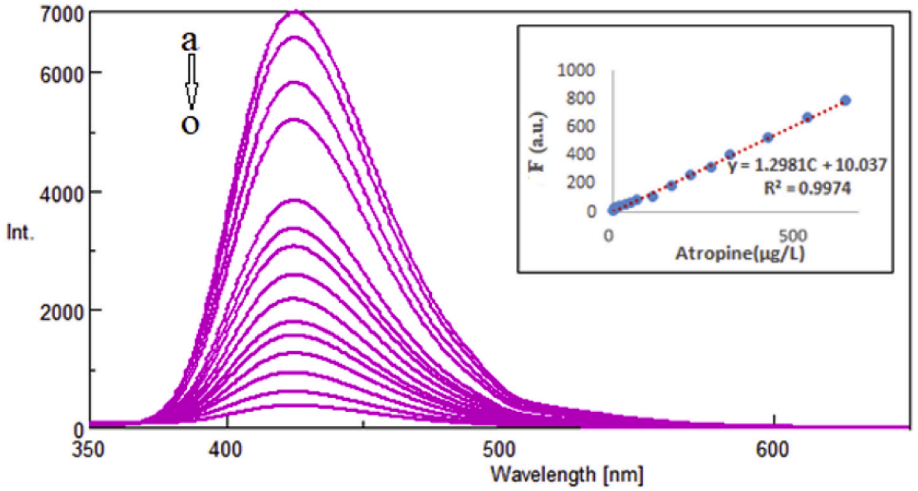

Fig. 10. Fluorescence spectra of TA–H_2O_2–Fe_3O_4@MOF/Dextrin composite solution in the presence of atropine with different concentrations [a–o: 1, 2, 5, 15, 30, 45, 60, 100, 150, 200, 250, 300, 400, 500, 600 μg L^{-1}, respectively].

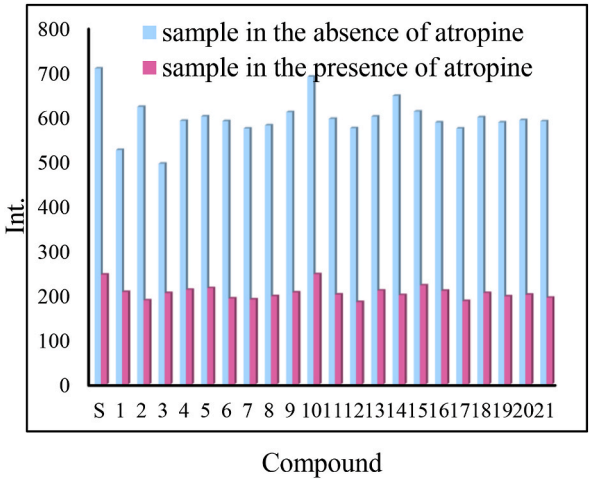

Fig. 11. The response of TA–H_2O_2– composite Fe_3O_4@MOF/Dextrin solution for different compounds in the absence or presence of atropine (optimum condition, atropine concentration is 100 μg L^{-1}, concentrations of other compounds are 20 time more than atropine), [S: main system, 1–21: leucine, glycine, L-histidine, L-serine, ascorbic acid, ampicillin, amoxicillin, alanine, L-cysteine, L-valine, codeine, L-arginine, cephalexin, vitamin B_2, L-lysine, glutathione, ibuprofen, methadone, glucose, lactose, uric acid, respectively].

diagnostic system for measuring Datura plant atropine extraction. This method has the lowest detection limit of 2.27 μg L^{-1} for measuring atropine in two types of D. Innoxia, D. Datura stramonium is north and west of Iran.

References

[1] P. Śramska, A. Maciejka, A. Topolewska, P. Stepnowski, Ł.P. Haliński, Isolation of atropine and scopolamine from plant material using liquid-liquid extraction and EXtrelut®columns, J. Chromatogr. B 1043 (2017) 202–208.
[2] M. Zhou, et al., Active fragments-guided drug discovery and design of selective tropane alkaloids using ultra-high performance liquid chromatography-quadrupole time-of-flight tandem mass spectrometry coupled with virtual calculation and biological evaluation, Anal. Bioanal. Chem. 409 (4) (2017) 1145–1157.
[3] I.M. De-la-Cruz, et al., Evolutionary response to herbivory: population differentiation in microsatellite loci, tropane alkaloids and leaf trichome density in Datura stramonium, Arthropod. Plant. Interact. 14 (1) (2020) 21–30.
[4] D.W. Robinson, et al., Datura quids at Pinwheel Cave, California, provide unambiguous confirmation of the ingestion of hallucinogens at a rock art site, Proc. Natl. Acad. Sci. USA 117 (49) (2020) 31026–31037.
[5] Y.S. Hui, et al., Identification and quantification of alkaloid compounds from different parts and production areas of datura metel l, Heterocycles an Int. J. Rev. Commun. Heterocycl. Chem. 100 (4) (2020) 568–584.
[6] K.I. Tapfuma, L. Mekuto, M.M. Makatini, V. Mavumengwana, The LC-QTOF-MS/MS analysis data of detected metabolites from the crude extract of Datura stramonium leaves, Data Brief 25 (2019), 104094.

[7] A. Moreno-Pedraza, J. Gabriel, H. Treutler, R. Winkler, F. Vergara, Effects of water availability in the soil on tropane alkaloid production in cultivated datura stramonium, Metabolites 9 (7) (2019) 131.
[8] C. Xia, et al., Characterization of the metabolic fate of Datura metel seed extract and its main constituents in rats, Front. Pharmacol. 10 (2019) 571.
[9] M. Cirlini, T.M. Demuth, A. Biancardi, M. Rychlik, C. Dall'Asta, R. Bruni, Are tropane alkaloids present in organic foods? Detection of scopolamine and atropine in organic buckwheat (Fagopyron esculentum L.) products by UHPLC–MS/MS, Food Chem. 239 (2018) 141–147.
[10] A. Zhang, C. Miao, H. Shi, H. Xiang, C. Huang, N. Jia, A novel solid-state electrochemiluminescence sensor for atropine determination based on Ru (bpy) 32+/ carbon nanospheres/Nafion composite film, Sens. Actuators, B 222 (2016) 433–439.
[11] N. Bagheri, B. Habibi, A. Khataee, J. Hassanzadeh, Application of surface molecular imprinted magnetic graphene oxide and high performance mimetic behavior of bi-metal ZnCo MOF for determination of atropine in human serum, Talanta 201 (2019) 286–294.
[12] J. Abbasifar, A. Samadi-Maybodi, Selective determination of atropine using poly dopamine-coated molecularly imprinted Mn-doped ZnS quantum dots, J. Fluoresc. 26 (5) (2016) 1645–1652.
[13] T. Mroczek, K. Głowniak, J. Kowalska, Solid–liquid extraction and cation-exchange solid-phase extraction using a mixed-mode polymeric sorbent of Datura and related alkaloids, J. Chromatogr. A 1107 (1–2) (2006) 9–18.
[14] S. Sun, J. Lu, Flow-injection post chemiluminescence determination of atropine sulfate, Anal. Chim. Acta 580 (1) (2006) 9–13.
[15] L. Chen, Q. Xu, Metal-organic framework composites for catalysis, Matter 1 (1) (2019) 57–89.
[16] S. Yuan, et al., Stable metal–organic frameworks: design, synthesis, and applications, Adv. Mater. 30 (37) (2018), 1704303.
[17] N.C. Burtch, J. Heinen, T.D. Bennett, D. Dubbeldam, M.D. Allendorf, Mechanical properties in metal–organic frameworks: emerging opportunities and challenges for device functionality and technological applications, Adv. Mater. 30 (37) (2018), 1704124.
[18] Y.-Z. Chen, Z.U. Wang, H. Wang, J. Lu, S.-H. Yu, H.-L. Jiang, Singlet oxygen-engaged selective photo-oxidation over Pt nanocrystals/porphyrinic MOF: the roles of photothermal effect and Pt electronic state, J. Am. Chem. Soc. 139 (5) (2017) 2035–2044.
[19] B. Li, J.-G. Ma, P. Cheng, Silica-protection-assisted encapsulation of Cu2O nanocubes into a metal–organic framework (ZIF-8) to provide a composite catalyst, Angew. Chem. 130 (23) (2018) 6950–6953.
[20] L. Chen, R. Luque, Y. Li, Encapsulation of metal nanostructures into metal–organic frameworks, Dalton Trans. 47 (11) (2018) 3663–3668.
[21] F. Chen, K. Shen, J. Chen, X. Yang, J. Cui, Y. Li, General immobilization of ultrafine alloyed nanoparticles within metal–organic frameworks with high loadings for advanced synergetic catalysis, ACS Cent. Sci. 5 (1) (2019) 176–185.
[22] J.P. Mehta, et al., Sol–gel synthesis of robust metal–organic frameworks for nanoparticle encapsulation, Adv. Funct. Mater. 28 (8) (2018), 1705588.
[23] Z.-C. Kong, et al., Core@ shell CsPbBr3@ zeolitic imidazolate framework nanocomposite for efficient photocatalytic CO2 reduction, ACS Energy Lett. 3 (11) (2018) 2656–2662.
[24] D.-M. Chen, X.-J. Zhang, A polyoxometalate template metal-organic framework with unusual ${$Cu8 ($μ$4-OH) 6$}$ 10+ secondary building unit for photocatalytic dye degradation, Inorg. Chem. Commun. 108 (2019), 107523.
[25] M. Ramesh, C. Deepa, Metal-organic frameworks and their composites, in: Metal-Organic Frameworks for Chemical Reactions, Elsevier, 2021, pp. 1–18.
[26] C.-D. Wu, M. Zhao, Incorporation of molecular catalysts in metal–organic frameworks for highly efficient heterogeneous catalysis, Adv. Mater. 29 (14) (2017), 1605446.
[27] Z. Li, T.M. Rayder, L. Luo, J.A. Byers, C.-K. Tsung, Aperture-opening encapsulation of a transition metal catalyst in a metal–organic framework for CO2 hydrogenation, J. Am. Chem. Soc. 140 (26) (2018) 8082–8085.
[28] W. Liang, et al., Metal–organic framework-based enzyme biocomposites, Chem. Rev. 121 (3) (2021) 1077–1129.
[29] R. Singh, M.M. Musameh, Y. Gao, B. Ozcelik, C.M. Doherty, "Stable MOF@ enzyme composites for electrochemical biosensing devices,", J. Mater. Chem. C (2021).
[30] C. Wang, L. Zhang, X. Li, A. Yu, S. Zhang, Controlled fabrication of core-shell silica@ chiral metal-organic framework for significant improvement chromatographic separation of enantiomers, Talanta 218 (2020), 121155.
[31] N. Yuan, X. Zhang, L. Wang, The marriage of metal–organic frameworks and silica materials for advanced applications, Coord. Chem. Rev. 421 (2020), 213442.
[32] M. Ding, H.-L. Jiang, Incorporation of imidazolium-based poly (ionic liquid) s into a metal–organic framework for CO2 capture and conversion, ACS Catal. 8 (4) (2018) 3194–3201.
[33] Y. Hou, et al., A review on metal-organic hybrids as flame retardants for enhancing fire safety of polymer composites, Compos. B Eng. (2021) 109014.
[34] M. Kalaj, et al., MOF-polymer hybrid materials: from simple composites to tailored architectures, Chem. Rev. 120 (16) (2020) 8267–8302.
[35] J.A. Khan, et al., Ultraviolet–visible light–sensitive high surface area phosphorous-fluorine–co-doped TiO2 nanoparticles for the degradation of atrazine in water, Environ. Eng. Sci. 31 (7) (2014) 435–446.
[36] J. Wang, et al., Superparamagnetic microsphere-assisted fluoroimmunoassay for rapid assessment of acute myocardial infarction, Biosens. Bioelectron. 24 (10) (2009) 3097–3102.
[37] A. V Biradar, V.S. Patil, P. Chandra, D.S. Doke, T. Asefa, A trifunctional mesoporous silica-based, highly active catalyst for one-pot, three-step cascade reactions, Chem. Commun. 51 (40) (2015) 8496–8499.
[38] A.H. Rezayan, M. Mousavi, S. Kheirjou, G. Amoabediny, M.S. Ardestani, J. Mohammadnejad, Monodisperse magnetite (Fe3O4) nanoparticles modified with water soluble polymers for the diagnosis of breast cancer by MRI method, J. Magn. Magn Mater. 420 (2016) 210–217.
[39] G. Ayoub, et al., Rational synthesis of mixed-metal microporous metal–organic frameworks with controlled composition using mechanochemistry, Chem. Mater. 31 (15) (2019) 5494–5501.
[40] J. Li, et al., Unprecedented highly efficient capture of glycopeptides by Fe 3 O 4@ Mg-MOF-74 core–shell nanoparticles, Chem. Commun. 53 (28) (2017) 4018–4021.
[41] Meteku B.E., Zeng J., Yan Z., Magnetic rod-based metal-organic frameworks metal 2 composites for colorimetric detection of hydrogen 3 peroxide (H2O2) and pollutant elimination 4 (2020).
[42] R. Han, et al., A simple chemiluminescent aptasensor for the detection of $α$-fetoprotein based on iron-based metal organic frameworks. New J. Chem. 44 (10) :4099–4107, 2020.
[43] H. Niu, Y. Zheng, S. Wang, L. Zhao, S. Yang, Y. Cai, Continuous generation of hydroxyl radicals for highly efficient elimination of chlorophenols and phenols catalyzed by heterogeneous Fenton-like catalysts yolk/shell Pd@ Fe3O4@ metal organic frameworks, J. Hazard. Mater 346 (2018) 174–183.
[44] H.-Q. Zheng, et al.Zr-based metal–organic frameworks with intrinsic peroxidase-like activity for ultradeep oxidative desulfurization: mechanism of H2O2 decomposition," Inorg. Chem. 58 (10):6983–6992, 2019.
[45] J. Wang, M. Bao, T. Wei, Z. Wang, Z. Dai, Bimetallic metal–organic framework for enzyme immobilization by biomimetic mineralization: Constructing a mimic enzyme and simultaneously immobilizing natural enzymes, Anal. Chim. Acta 1098 (2020) 148–154.
[46] H. Yang, R. Yang, P. Zhang, Y. Qin, T. Chen, F. Ye, A bimetallic (Co/2Fe) metal-organic framework with oxidase and peroxidase mimicking activity for colorimetric detection of hydrogen peroxide, Microchim. Acta. 184 (12) (2017) 4629–4635.
[47] Z. Qi, L. Wang, Q. You, Y. Chen, PA-Tb-Cu MOF as luminescent nanoenzyme for catalytic assay of hydrogen peroxide, *Biosens. Bioelectron.* 96 (2017) 227–232.
[48] T. Wu, et al., Colorimetric detection of ascorbic acid and alkaline phosphatase activity based on the novel oxidase mimetic of Fe–Co bimetallic alloy encapsulated porous carbon nanocages, *Talanta* 202 (2019) 354–361.
[49] M. Sayed, et al., Bismuth-doped nano zerovalent iron: a novel catalyst for chloramphenicol degradation and hydrogen production, ACS Omega 5 (47) (2020) 30610–30624.
[50] M. Sayed, et al., In-situ dual applications of ionic liquid coated Co2+ and Fe3+ co-doped TiO2: superior photocatalytic degradation of ofloxacin at pilot scale level and enhanced peroxidase like activity for calorimetric biosensing, J. Mol. Liq. 282 (2019) 275–285.

[51] M. Sayed, et al., Narrowing the band gap of TiO2 by co-doping with Mn2+ and Co2+ for efficient photocatalytic degradation of enoxacin and its additional peroxidase like activity: a mechanistic approach, J. Mol. Liq. 272 (2018) 403–412.
[52] J. Wang, et al., Superparamagnetic microsphere-assisted fluoroimmunoassay for rapid assessment of acute myocardial infarction, *Biosens. Bioelectron.* 24 (10) (2009) 3097–3102.
[53] A. V Biradar, V.S. Patil, P. Chandra, D.S. Doke, T. Asefa, A trifunctional mesoporous silica-based, highly active catalyst for one-pot, three-step cascade reactions, *Chem. Commun.* 51 (40) (2015) 8496–8499.